Surface & Coatings Technology 312 (2017) 66–74

Contents lists available at ScienceDirect

Surface & Coatings Technology

journal homepage: www.elsevier.com/locate/surfcoat

Effects of diamond-like carbon film on the corrosion behavior of NdFeB permanent magnet

Hao Wu [a], Shu Xiao [a,b], Donglai Chen [a], Abdul Mateen Qasim [a], Kejian Ding [c], Guosong Wu [a], Paul K. Chu [a,*]

[a] Department of Physics and Materials Science, City University of Hong Kong, Tat Chee Avenue, Kowloon, Hong Kong, China
[b] School of Advanced Materials, Shenzhen Graduate School, Peking University, Shenzhen 518055, China
[c] Department of Biological Science and Technology, Beijing Jiao Tong University, Beijing 100044, China

ARTICLE INFO

Article history:
Received 16 June 2016
Revised 16 August 2016
Accepted in revised form 7 September 2016
Available online 9 September 2016

Keywords:
Rare earth elements
Permanent magnet
Diamond-like carbon
Corrosion
EIS

ABSTRACT

A diamond-like carbon (DLC) film is deposited on the NdFeB permanent magnet by plasma immersion ion implantation and deposition (PIII&D) and characterized by atomic force microscopy, scanning electron microscopy, Raman scattering, and mechanical tests. Electrochemical and immersion tests conducted for different time durations show that the corrosion resistance in 3.5% NaCl and 5 mM H_2SO_4 is improved by the DLC coating and corrosion tests also reveal enhanced corrosion resistance in both media. The corrosion mechanism of both the untreated and DLC-coated NdFeB is proposed and discussed.

1. Introduction

Owing to the excellent magnetic properties, Nd-Fe-B (NFB) permanent magnets have diverse applications, especially in the electronics industry. However, the poor intrinsic corrosion resistance of NdFeB magnets severely hinders practical applications and deposition of surface coatings and alloying have been proposed to improve the corrosion properties of NdFeB [1–5]. Various kinds of coatings have been applied to improve the corrosion resistance of NdFeB, for instance, Al [6], Al/Al_2O_3 [7], Ti/Al [8], Ti/TiN [9], Ni [10], silane [11], phosphate [12], NiP [13], Ni-TiO_2 composites [14], graphene oxide [15], and acrylic polymer composites [16,17]. Different methods such as magnetron sputtering [6–9], ion beam sputtering [10], electrochemical deposition [13–16], and chemical conversion [18–20] have been employed to form these protective coatings on NdFeB.

Diamond-like carbon (DLC), an allotrope consisting of amorphous carbon with a significant fraction of sp^3 bonds, has high mechanical hardness and chemical inertness [21,22] and is often used in corrosion mitigation and prevention [23–25]. However, it is difficult to fabricate DLC coatings with good adhesion on some substrates. Pre-deposited intermediate layers have been used to improve the adhesion but concomitant problems such as galvanic effects may be introduced thereby adversely affecting the corrosion resistance [26]. Plasma immersion ion implantation and deposition (PIII&D) is an advanced surface modification technique combining energetic ion implantation and low-energy plasma deposition [27,28]. The bonding strength between the substrate and coating can be increased by means of energetic bombardment which can also be used to clean the sample surface prior to deposition [29]. In this work, a DLC film is deposited on NdFeB by PIII&D and the corrosion behavior of the untreated and DLC-coated NdFeB (NdFeB-DLC) is investigated in NaCl and H_2SO_4.

2. Experimental details

Sintered NdFeB magnets with dimensions of 10 mm × 10 mm × 5 mm were ground and polished with up to #4000 SiC paper and ultrasonically cleaned in alcohol. PIII&D was conducted at a base pressure of 2×10^{-3} Pa. C_2H_2 was bled into the chamber at a flow rate of 30 sccm and the plasma was sustained with 450 W radio frequency (RF). A pulsed bias voltage (20 kV, pulse width of 50 μs, and pulsing frequency of 100 Hz) was applied to the NdFeB sample for 3 h to conduct deposition.

Atomic force microscopy (AFM, Auto Probe CP, Park Scientific Instruments, USA) was used to assess the sample surface morphology of the samples before and after plasma modification and the Raman scattering spectra were acquired using a 514.5 nm argon laser (Horiba LabRAM). Scanning electron microscopy (SEM) was performed to examine the surface and cross-sectional morphology and energy dispersive X-ray spectrometry (EDS) was employed to determine the elemental composition in the line scan mode. A Teer 3001 scratch tester with a 0.2 mm radius diamond indenter was used to perform the scratch test and the

* Corresponding author.
E-mail address: paul.chu@cityu.edu.hk (P.K. Chu).

http://dx.doi.org/10.1016/j.surfcoat.2016.09.008
0257-8972/

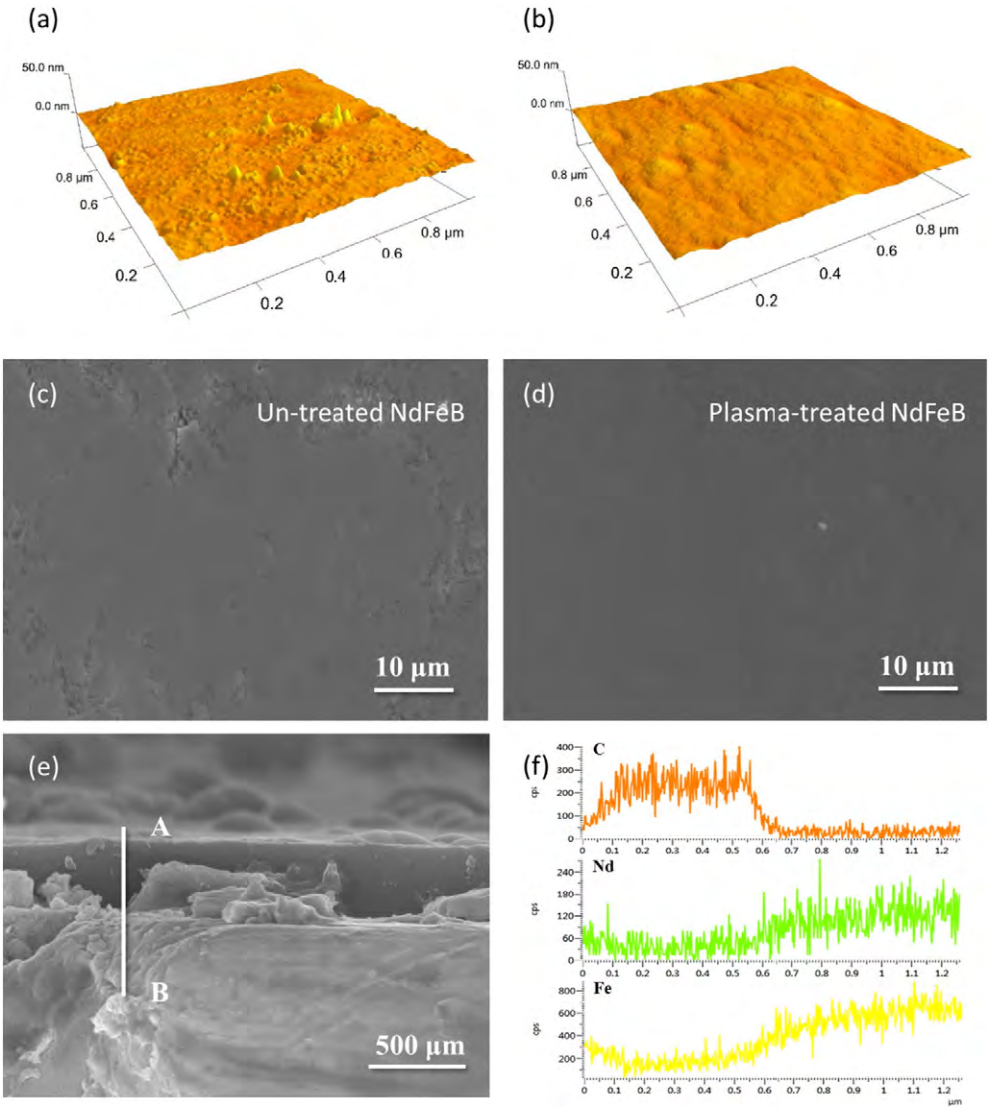

Fig. 1. AFM images (1 × 1 μm) of (a) NdFeB and (b) Plasma-treated NdFeB samples; Surface morphology of (c) NdFeB and (d) Plasma-treated NdFeB samples at ×2000 magnification; (e) Cross-sectional image of the plasma-treated NdFeB sample; (f) EDS line scan of the deposited film.

measurement was carried out at a loading rate of 50 N/min and linear speed of 5 mm/min. An MTS nano-indenter was utilized to determine the hardness and elastic modulus using the continuous stiffness measurement (CSM) mode.

The corrosion behavior of the untreated and implanted NdFeB samples was evaluated in 3.5% NaCl and 5 mM H_2SO_4 at 25 °C. The electrochemical experiments were conducted on a Zahner Zennium electrochemical workstation based on the three-electrode technique. A platinum sheet and Ag/AgCl electrode were used as the counter electrode and reference electrode, respectively. The specimen with a surface area of 0.5 cm^2 was exposed to the solution. Potentiodynamic polarization was performed at a scanning rate of 1 mV/s from −250 mV in the cathodic direction to +500 mV in the anodic direction based on the open circuit potentials (OCPs) after immersion for 30 min. The electrochemical impedance spectra (EIS) were collected at the respective OCPs after stabilization in the solution for 30 min. Immersion experiments were carried out to evaluate the corrosion behavior of both the NdFeB and NdFeB-DLC samples. After immersion in 3.5% NaCl and 5 mM H_2SO_4 for 1 h and 24 h, the surface morphology of the corroded samples was observed by SEM. The cross-sectional images were also acquired after immersion for 24.

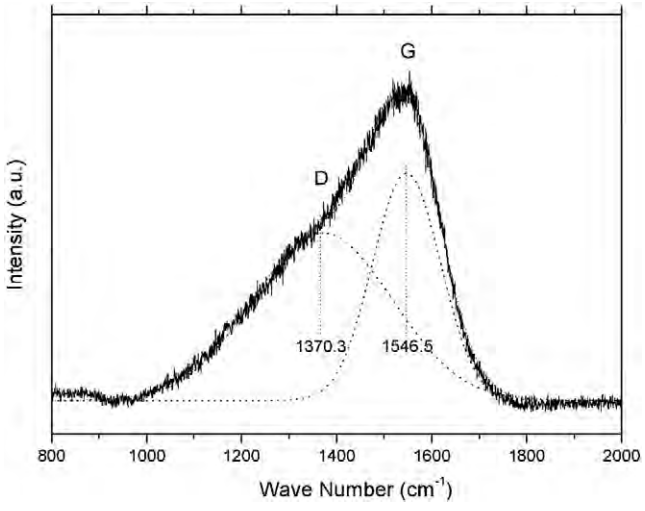

Fig. 2. Raman spectrum acquired from the DLC film.

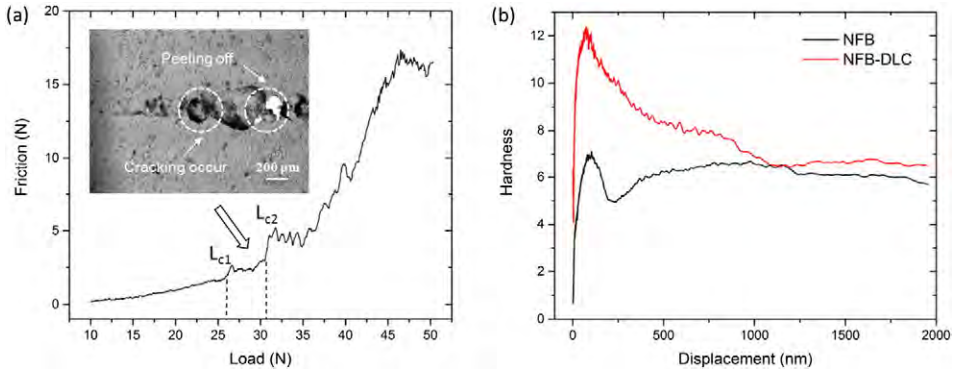

Fig. 3. (a) Frictional plot for the scratch test of DLC film on NdFeB with the inset shows optical microscope image of film failure in the scratch test; (b) Hardness of the NdFeB and NdFeB-DLC samples as a function of displacement.

Table 1
E_{cor}, I_{cor}, and β_c of NdFeB and NdFeB-DLC in 3.5% NaCl and 5 mM H_2SO_4 derived from the polarization curves.

	3.5% NaCl		5 mM H_2SO_4	
	NdFeB	NdFeB-DLC	NdFeB	NdFeB-DLC
E_{cor} (V, vs Ag/AgCl)	−0.70 ± 0.02	−0.64 ± 0.05	−0.66 ± 0.01	−0.62 ± 0.01
I_{cor} (mA/cm^2)	8.9 ± 0.8	2.8 ± 0.3	232 ± 14.8	19.4 ± 1.7
β_c (V/decade)	−0.231 ± 0.031	−0.28 ± 0.059	−0.304 ± 0.01	−0.613 ± 0.079

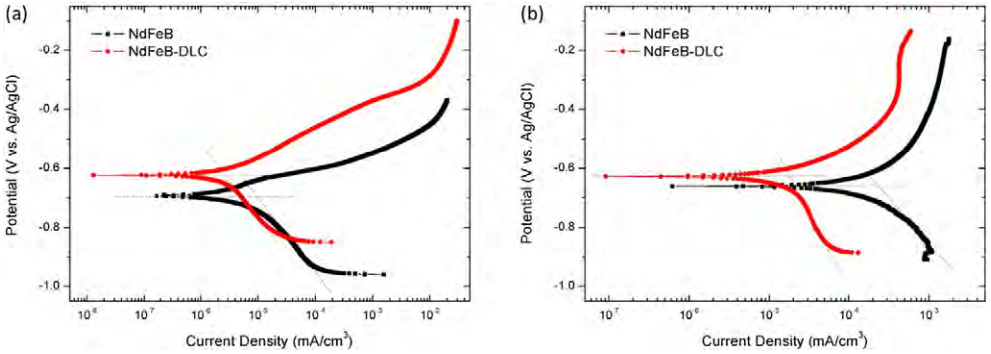

Fig. 4. Polarization curves of NdFeB and NdFeB-DLC sample in (a) 3.5% NaCl and (b) 5 mM H_2SO_4.

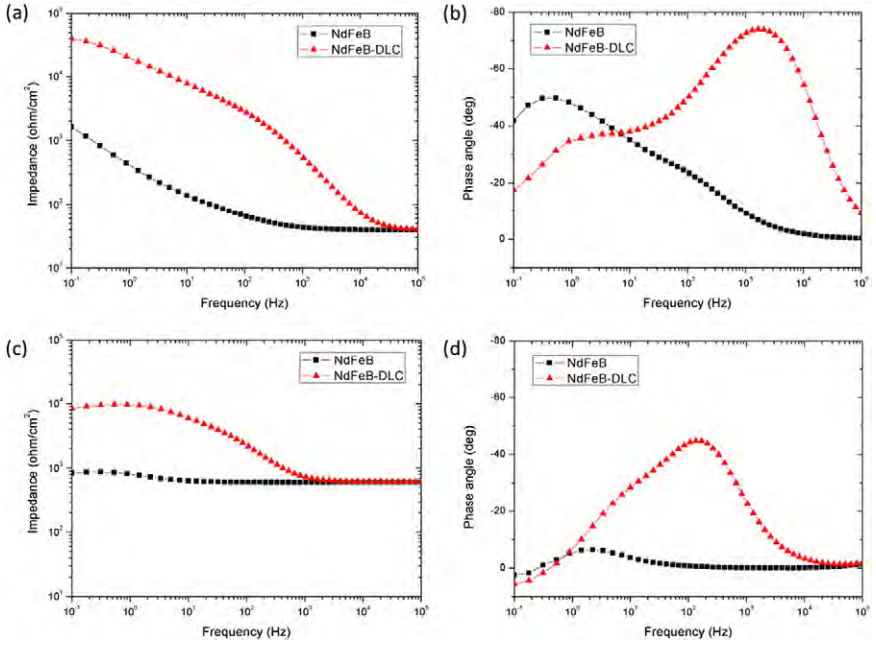

Fig. 5. (a and c) Bode impedance and (b and d) Bode phase angle plots of NdFeB and NdFeB-DLC after immersion for 30 min in (a, b) 3.5% NaCl and (c, d) 5 mM H_2SO_4 at room temperature.

Table 2
Fitted EIS results of NdFeB and NdFeB-DLC in 3.5% NaCl and 5 mM H_2SO_4 based on the corresponding equivalent circuit models.

	3.5% NaCl		5 mM H_2SO_4	
	NdFeB	NdFeB-DLC	NdFeB	NdFeB-DLC
R_s (ohm $*$ cm^{-2})	38.71 ± 0.11	39.45 ± 0.06	603 ± 1.1	609.6 ± 1.3
Y_f (ohm^{-2} $*$ cm^{-2} $*$ S^{-n})	–	$(3.965 \pm 0.2) \times 10^{-5}$	–	–
n_f	–	0.9857 ± 0.0272	–	–
R_{pore} (ohm $*$ cm^{-2})	–	9283 ± 99.3	–	–
Y_{dl} (ohm^{-2} $*$ cm^{-2} $*$ S^{-n})	$(5.152 \pm 0.3807) \times 10^{-3}$	$(3.158 \pm 0.037) \times 10^{-7}$	$(4.792 \pm 0.356) \times 10^{-4}$	$(1.3 \pm 0.05) \times 10^{-6}$
n_{dl}	0.6657 ± 0.0126	0.9829 ± 0.0012	0.832 ± 0.022	0.8976 ± 0.0047
R_{ct} (ohm $*$ cm^{-2})	60.24 ± 4.68	1734 ± 57	293 ± 9.7	4234 ± 132
Y_{diff} (ohm^{-2} $*$ cm^{-2} $*$ S^{-n})	$(7.245 \pm 0.072) \times 10^{-4}$	$(2.089 \pm 0.059) \times 10^{-5}$	–	$(1.002 \pm 0.055) \times 10^{-5}$
n_{diff}	0.7106 ± 0.0085	0.4522 ± 0.0058	–	0.7849 ± 0.0202
R_{diff} (ohm $*$ cm^{-2})	4269 ± 208	$(5.421 \pm 0.0156) \times 10^4$	–	5395 ± 194
R_L (ohm $*$ cm^{-2})	–	–	329.4 ± 85.5	7993 ± 666
I (Henri $*$ cm^{-2})	–	–	1060 ± 133	$(1.119 \pm 0.069) \times 10^4$
χ^2	1.075×10^{-4}	1.082×10^{-5}	6.334×10^{-5}	6.384×10^{-5}

3. Result and discussion

The AFM images of the untreated and plasma-treated NdFeB samples are shown in Fig. 1. Fig. 1(a) shows some localized bud-like protrusions on the untreated NdFeB sample and the plasma-treated NdFeB sample reveals a smoother surface morphology with the average surface roughness decreasing from 1.06 nm to 0.92 nm, indicating that the sample roughness is reduced by energetic ion bombardment and coating formation. The samples are also characterized by SEM. As shown in Fig. 1(c) and 1(d), the polished NdFeB sample has a relatively rough surface with some randomly distributed defects. After PIII&D, a more uniform and flat surface is observed. The cross sectional micrograph of the plasma-treated NdFeB sample is displayed in Fig. 1(e). A dense and continuous film with an average thickness of about 500 nm can be observed and the EDS line scan obtained from point A to point B in Fig. 1 (e) confirms that it is composed of carbon.

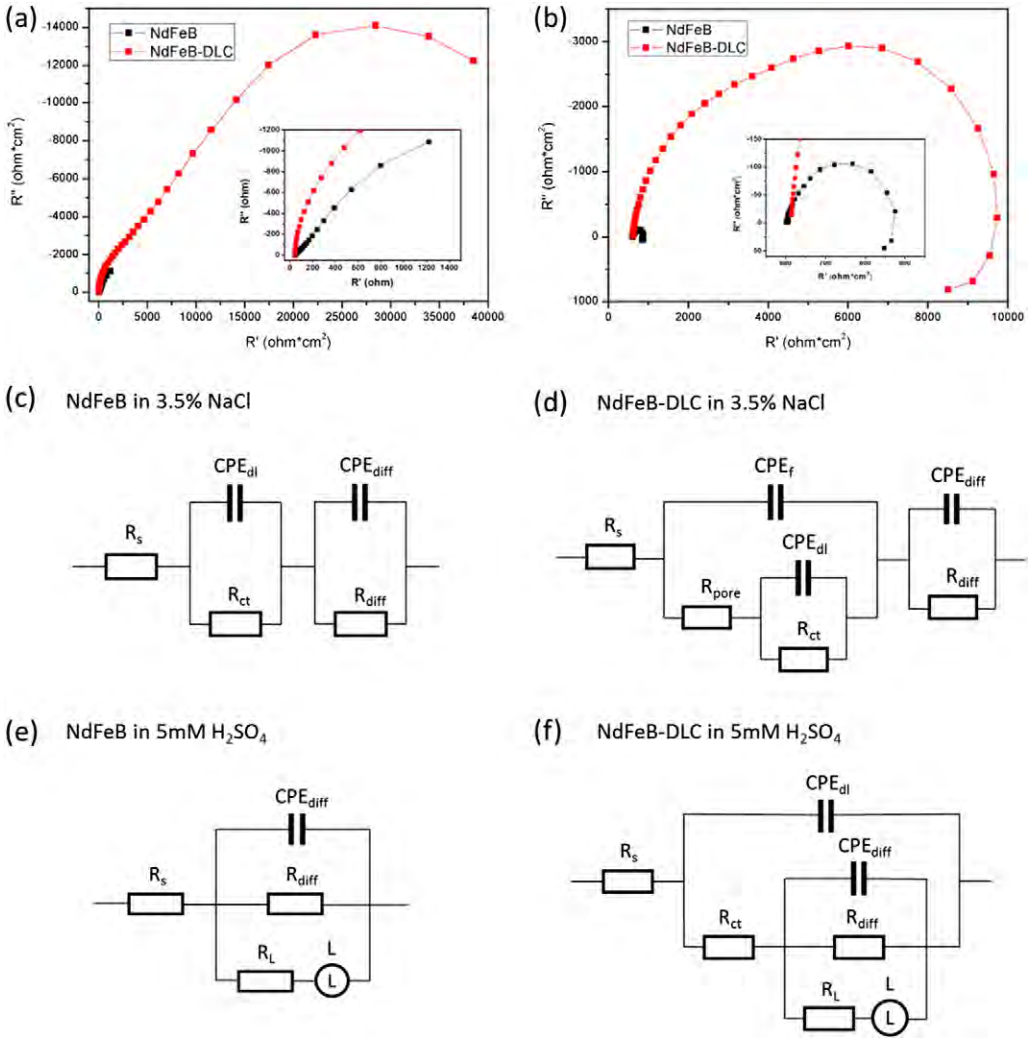

Fig. 6. Nyquist plots of NdFeB and NdFeB-DLC after immersion for 30 min in (a) 3.5% NaCl and (b) 5 mM H_2SO_4 at room temperature, with the electrochemical equivalent circuit used to fit the impedance spectra of: (c) NdFeB in 3.5% NaCl; (d) NdFeB-DLC in 3.5% NaCl; (e) NdFeB in 5 mM H_2SO_4 and (f) NdFeB-DLC in 5 mM H_2SO_4.

Raman scattering is performed to characterize the PIII&D sample. As shown in Fig. 2, a typical diamond-like carbon (DLC) pattern is observed. The Raman spectrum can be deconvoluted into two subpeaks: D band at 1370.3 cm^{-1} and G band at 1546.5 cm^{-1} with an I_D/I_G ratio of 1.2. The G band arises from stretching of sp^2 atoms in both rings and chains [30] and D band is due to the breathing modes of sp^2 atoms in the rings [31]. The I_D/I_G ratio is related to the order of the sp^2 configuration and sp^2/sp^3 fraction ratio [32,33]. During PIII&D, C_2H_2 is first ionized into carbon and hydrocarbon ions by the RF and the film-forming plasma is accelerated to the sample surface by a voltage of 25 kV. Energetic ion bombardment results in implantation as well as formation of sp^3 in the DLC film [34,35]. High-energy ion implantation also induces inter-diffusion and improves the adhesion between the film and substrate [36]. Adhesion and hardness tests are conducted on the DLC sample. In the adhesion test, the critical loading (L_c) is measured by the inflection point in the frictional force curve and observation of film failure [37]. The load at which the first crack occurs is referred to as the lower critical load L_{c1} and that corresponding to film delamination is designated the higher critical load L_{c2} [38]. As shown in Fig. 3(a), the friction plot shows an L_{c1} of 25.9 N and L_{c2} of 30.5 N, which also match the optical observation of film failure in the scratch test. The result indicates that the DLC film has decent adhesion with the substrate without an intermediate layer. However, the crack propagation resistance of the as-deposited DLC film is not very good and it may be due to film defects caused by the intrinsically uneven surface morphology of the NdFeB substrate. As shown in Fig. 3(b), the hardness of the DLC-coated sample decreases gradually with indentation displacement finally reaching a value comparable to that of the NdFeB substrate, indicating that the surface mechanical property of the NdFeB sample is improved with the DLC coating.

The potentiodynamic polarization curves acquired from NdFeB and NdFeB-DLC in 3.5% NaCl and 5 mM H_2SO_4 are displayed in Fig. 4. The beginning of the anode section in the polarization curves is related to active dissolution and the anodic current density increases quickly with anode potentials. The E_{cor}, I_{cor}, and β_c values are calculated by Tafel extrapolation from the linear cathodic polarization region and the results are summarized in Table. 1. After DLC deposition, E_{cor} shifts towards the noble direction in both 3.5% NaCl and 5 mM H_2SO_4. The corrosion current density is one of the important parameters in corrosion rate determination. Compared to NdFeB, I_{cor} of NdFeB-DLC decreases 3.2 times in 3.5% NaCl from 8.9 mA/cm^3 to 2.8 mA/cm^3 and 12 times in 5 mM H_2SO_4 from 232 mA/cm^3 to 19.4 mA/cm^3. The results indicate that the DLC film improves the corrosion resistance of NdFeB, especially in 5 mM H_2SO_4.

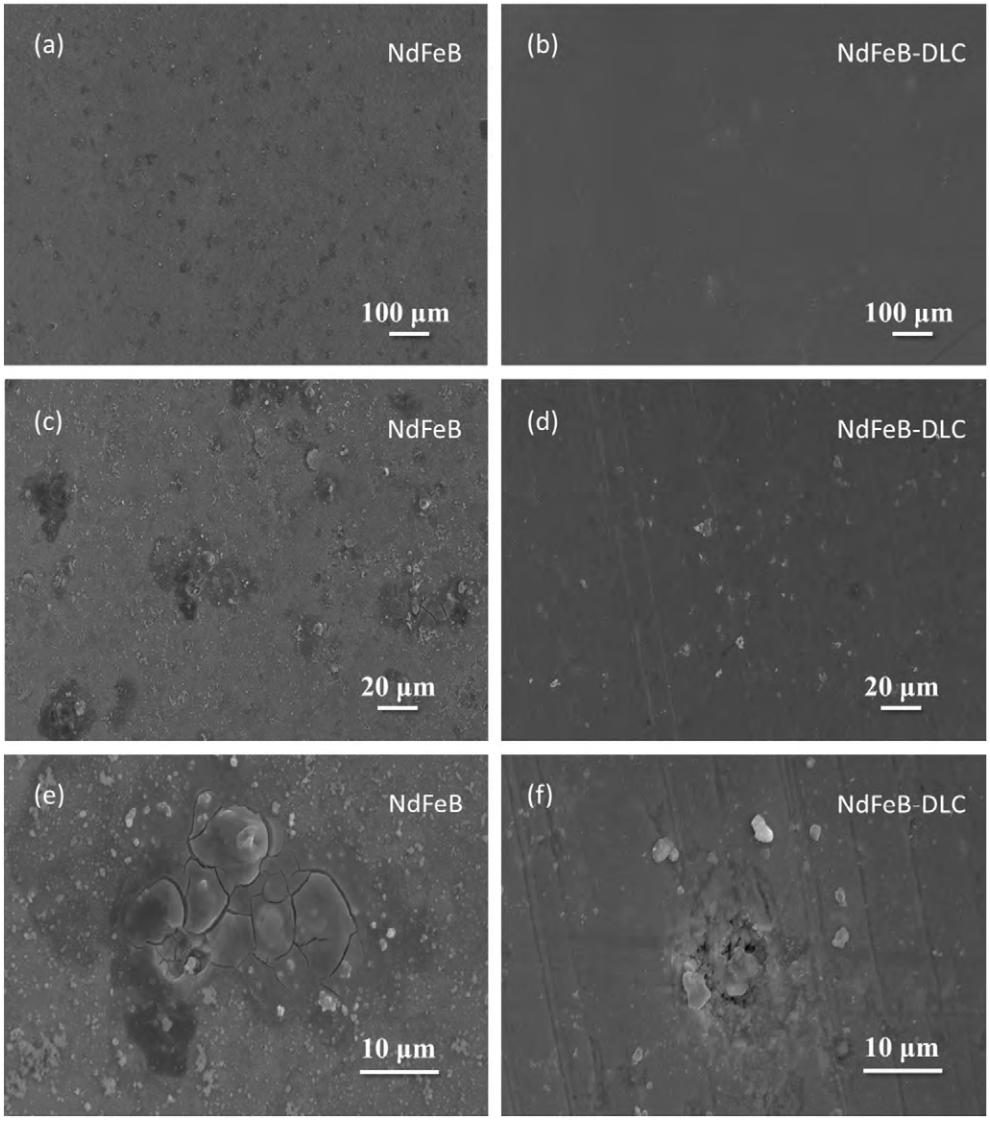

Fig. 7. Surface morphologies of NdFeB and NdFeB-DLC after immersion in 3.5% NaCl for 1 h.

To further investigate the corrosion process, EIS spectra are acquired from NdFeB and NdFeB-DLC after immersion in 3.5% NaCl and 5 mM H_2SO_4 for 30 min. The Bode impedance and Bode phase angle plots are displayed in Fig. 5. As shown in Fig. 5(a) and 5(c), the impedance of NdFeB-DLC is larger than that of NdFeB in both NaCl and H_2SO_4 at all frequencies. The impedance at low frequencies is an appropriate parameter to evaluate the protective properties. A larger impedance at low frequencies corresponds to better protective performance because it corresponds to the resistance against mass transportation of the dissolved ions [39]. The remarkable increase in the impedance in the low frequency region observed from NdFeB-DLC implies significantly improved corrosion resistance in the corrosive media. The phase angle also changes after the plasma treatment. In both NaCl and H_2SO_4, the untreated sample has a larger phase angle in the low-frequency region, whereas NdFeB-DLC shows a larger phase angle in the high-frequency region. The phase angle peak at higher frequencies is related to the formation of the surface film on the electrode surface and a larger maximum phase angle corresponds to better corrosion resistance. The maximum phase angle also changes from −50 to −74 in NaCl and −6 to −50 in H_2SO_4 after DLC deposition, respectively. The larger phase angle corresponds to a more capacitive response which indicates that penetration of the corrosive solution through the film or corrosion product layer to the substrate is weaker and the current becomes less significant.

The Nyquist plots are shown in Fig. 6. The capacitive loops in the Nyquist plots can be attributed to the surface film, charge transfer, and mass transfer in the corrosion product layer [40]. The capacitive loop in the higher-frequency region is associated with the charge transfer resistance during electron transfer in the Faradic process parallel to the double layer capacitance at the interface between the substrate and solution [41]. The low-frequency capacitive loop can be attributed to film formation and ion diffusion [42]. A parallel combination of the diffusion capacitance and resistance is introduced to describe the "finite-layer diffusion" process or heterogeneous penetration of an electrolyte [28]. In our study, a constant phase element (CPE) that represents a non-ideal capacitor is used to replace the capacitor C based on the Nyquist plots as follows [39]:

$$Y = Y_0(jw)^n \quad (1)$$

where j is the imaginary number and ω is the angular frequency. Y_0 and n are defined as the admittance constant and empirical exponent of the CPE, respectively.

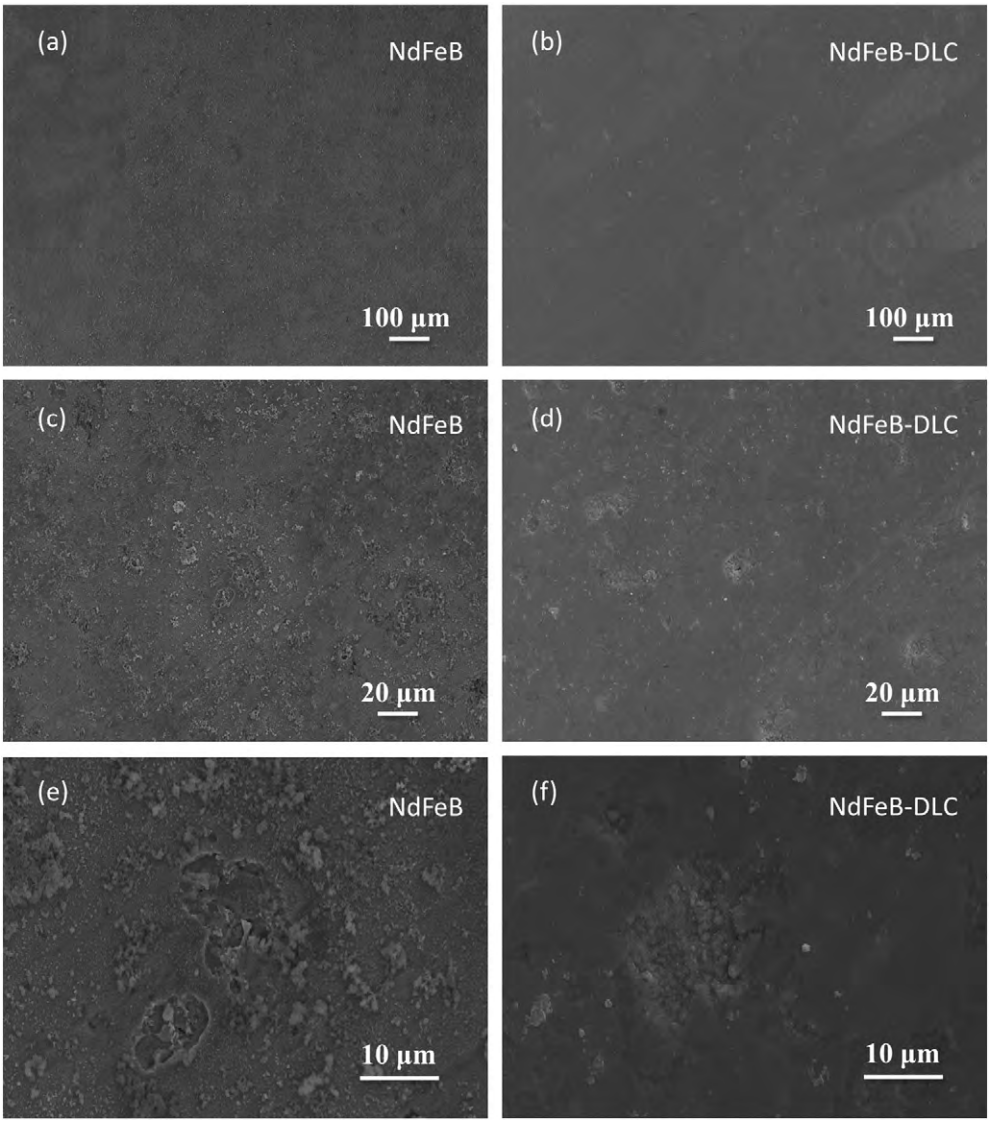

Fig. 8. Surface morphologies of NdFeB and NdFeB-DLC after immersion in 3.5% NaCl for 24 h.

As shown by the Bode phase angle plot (Fig. 5b) and Nyquist plot (Fig. 6a) in 3.5% NaCl, both NdFeB and NdFeB-DLC have two time constants within the range of our measurement. Two different equivalent circuit models (Fig. 6c and d) are established to fit the EIS data of NdFeB and NdFeB-DLC. With respect to NdFeB in 3.5% NaCl, an equivalent circuit $R_s(CPE_{dl}R_{ct})(CPE_{diff}R_{diff})$ is utilized to fit the Nyquist plot of NdFeB. With regard to NdFeB-DLC in NaCl, the equivalent circuit $R_s(CPE_f(R_{pore}(CPE_{dl}R_{ct})))(CPE_{diff}R_{diff})$ is employed to simulate the Nyquist plot of NdFeB-DLC. In the two circuits, R_s represents the solution resistance. CPE_f is the capacitance of the deposited film and R_{pore} is the sum of the resistance of all the pores in the film. CPE_{dl} represents the capacitance of the electrical double layer, and R_{ct} represents the related charge transfer resistance in the faradic process. CPE_{diff} represents the capacitance induced by ion diffusion, and R_{diff} represents the related ion diffusion resistance. The corrosion mechanism in 5 mM H_2SO_4 is different from that in the neutral NaCl solution. As shown in Fig. 6(e) and 6(f), $R_s(CPE_{diff}R_{diff}(LR_L))$ is used to simulate the corrosion behavior of NdFeB in 5 mM H_2SO_4 and $R_s(CPE_{dl}(R_{ct}(CPE_{diff}R_{diff}(LR_L))))$ is used for NdFeB-DLC. Here, the inductance L is introduced due to absorption of intermediate species during the corrosion process and R_L is related to the resistance related to the inductance. As shown in the simulated result, the diffusion resistance at low frequencies is the primary resistance and the charge transfer resistance in neglected. This stems from the reaction between sulfuric acid and NdFeB rendering reactant diffusion the dominating process in the corrosion process of NdFeB in sulfuric acid. The fitted EIS results based on these corresponding equivalent circuits are shown in Table 2. The polarization resistance R_p is evaluated by the sum of R_{diff}, R_{pore} and R_{ct} and proposed to evaluate the corrosion resistance. The results clearly confirm that the corrosion resistance of NdFeB in both neutral NaCl and acidic H_2SO_4 is improved by the DLC coating. This improvement can be attributed to the good barrier effect and insulating property of the DLC coating.

Immersion tests are conducted to investigate the corrosion behavior in the corrosive solutions. Figs. 7-10 show the surface morphologies of NdFeB and NdFeB-DLC after immersion in 3.5% NaCl and 5 mM H_2SO_4. After immersion in 3.5% NaCl for 1 h, extensive pitting holes and crevices can be observed from the untreated NdFeB sample but in contrast, only few pitting regions can be seen from the surface of NdFeB-DLC. These pitting regions can be attributed to the imperfection of the DLC coating which can be induced by preexisting defects on the NdFeB surface and film deposition process. The coating consists of a typical columnar growth structure and void defects are easily formed due to atomic shadowing [43,44]. In the corrosion process, the corrosion media may penetrate these defects causing pitting corrosion. After immersion in 3.5% NaCl for 24 h, severe corrosion manifested by enlarged corroded regions and precipitated corrosion products can been observed from

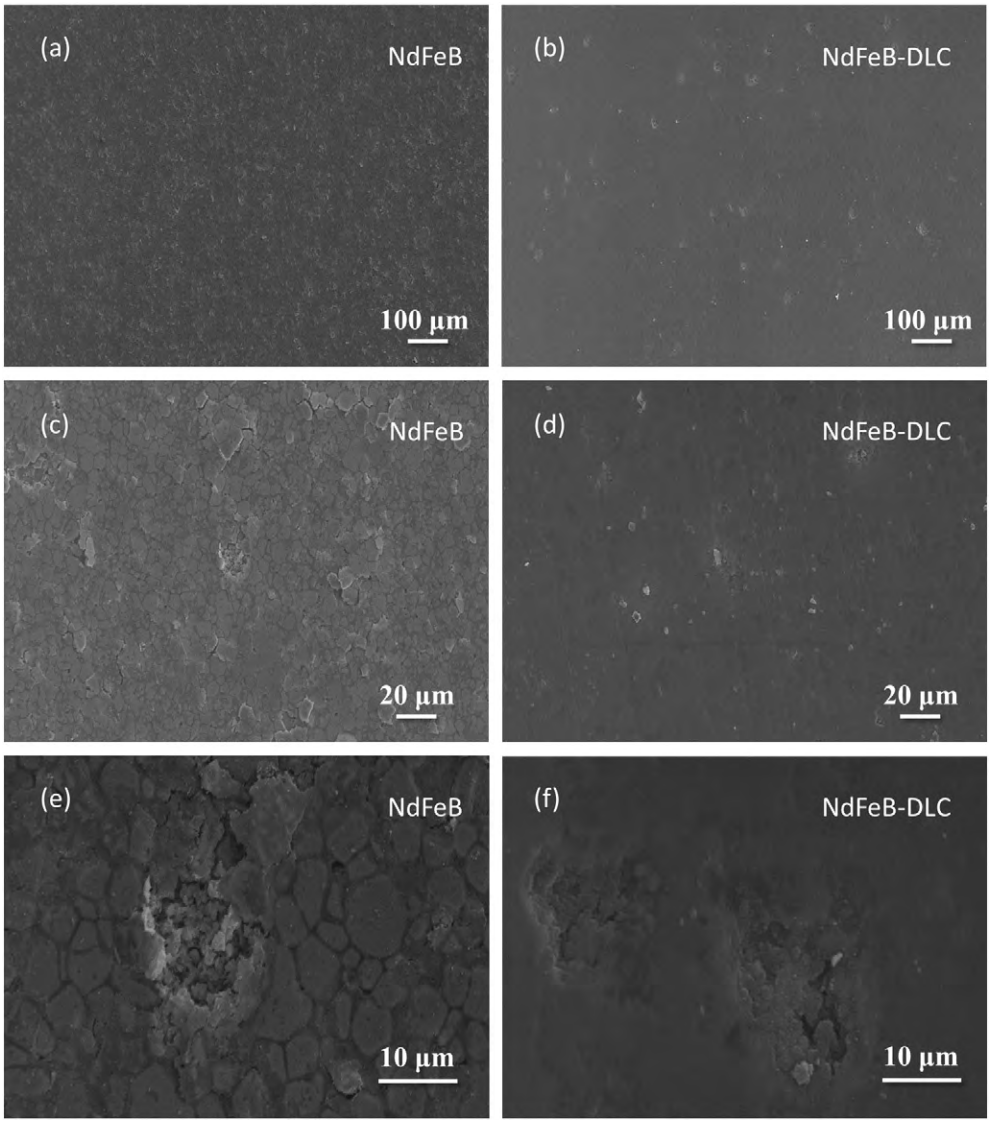

Fig. 9. Surface morphologies of NdFeB and NdFeB-DLC after immersion in 5 mM H_2SO_4 for 1 h.

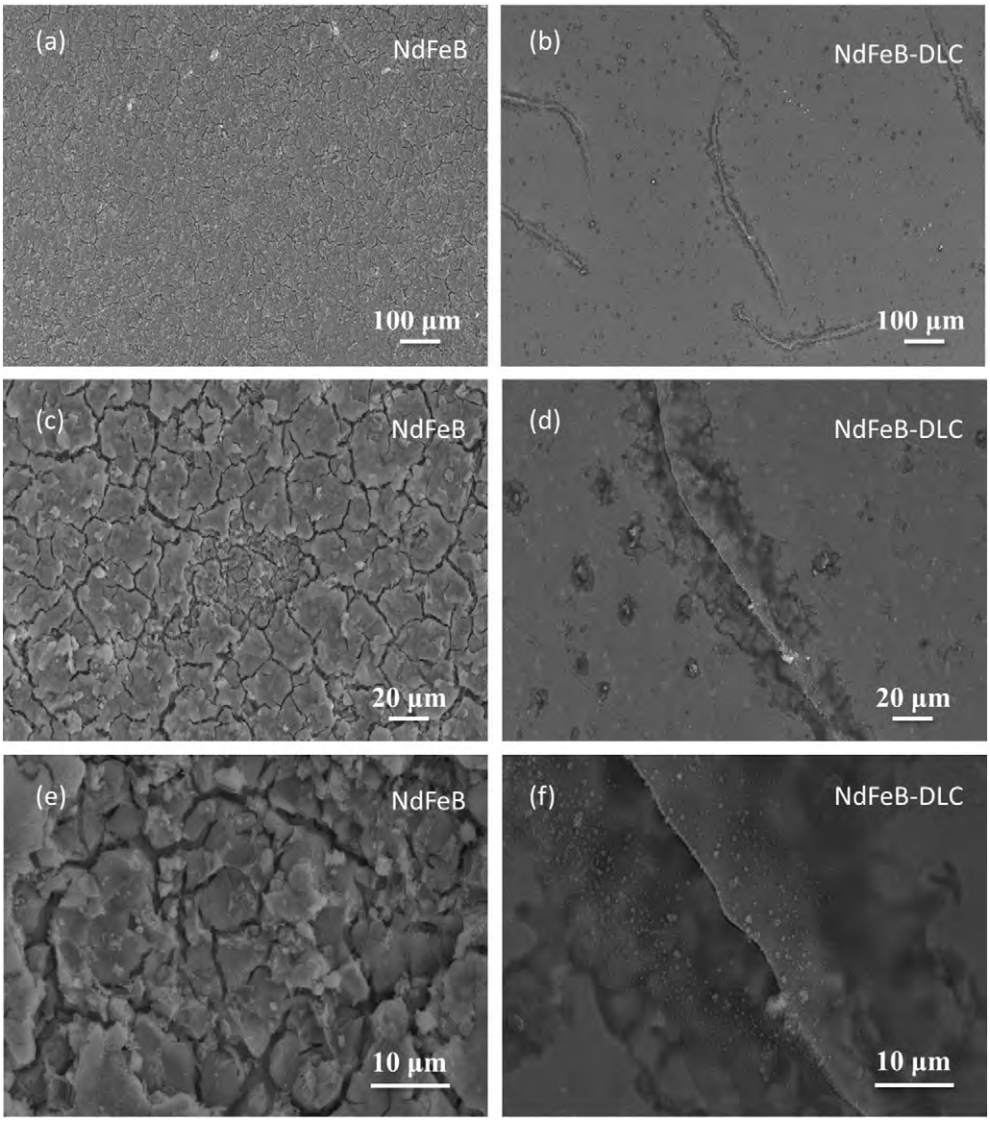

Fig. 10. Surface morphologies of NdFeB and NdFeB-DLC after immersion in 5 mM H_2SO_4 for 24 h.

the untreated NdFeB surface. However, the surface morphology of NdFeB-DLC does not change appreciably although the immersion time is increased from 1 h to 24 h, indicating that the DLC coating offers stable protection.

As shown in Figs. 9 and 10, after exposure to H_2SO_4 for 1 h, the NdFeB sample displays a typically acid-corroded surface with emerging grain boundaries and severe localized corrosion is observed. The NdFeB magnet typically comprises of three phases, the ferromagnetic phase matrix and corrosion sensitive Nd- and B-rich intergranular phases [2]. The grain boundary regions in the sintered NdFeB sample have mostly the Nd- and B-rich phases which have a larger electrostatic surface potential than the $Nd_2Fe_{14}B$ matrix phase and this can causes galvanic effects to accelerate preferential corrosion of the intergranular phase [45]. Therefore, the corrosion process on NdFeB can be described as preferential dissolution of the intergranular phases followed by separation of ferromagnetic grains from the surface before dissolution [46]. It has been reported that the Nd-rich phase in NdFeB dissolves anodically along the grain boundaries in concert with hydrogen generation in the corrosion process of sintered NdFeB [47,48]. With regard to NdFeB-DLC after immersion in H_2SO_4 for 1 h, only few pitting regions can be observed from the surface. After immersion in H_2SO_4 for 24 h, the NdFeB sample shows a cracked morphology with web-like corrosion crevices and subsequent grain detachment can be observed due to embrittlement of NdFeB surface. With respect to NdFeB-DLC, some pitting and cracks can be observed after immersion in sulfuric acid for 24 h. These pitting and cracks arise from defects generated during the formation of the DLC film. However, most of the DLC coating remains flat and integrated without much destruction. All in all, our results indicate that the DLC film formed by PIII&D results in improved corrosion resistance of NdFeB in both neutral NaCl and acidic H_2SO_4 solutions.

4. Conclusion

Plasma immersion ion implantation and deposition is performed to deposit a DLC film on the NdFeB magnet. The electrochemical and immersion corrosion results show that the corrosion resistance in neutral 3.5% NaCl and 5 mM H_2SO_4 solutions are significantly improved by the DLC coating which has good barrier properties. However, some preexisting defects in the film may induce local film cracking and subsequent corrosion failure in the solutions, especially in sulfuric acid. Hence, the original film quality must be maintained in order to achieve good corrosion resistance.

Acknowledgements

The work was financially supported by Hong Kong Research Grants Council (RGC) General Research Funds (GRF) No. CityU 11301215.

References

[1] J. Jacobson, A. Kim, J. Appl. Phys. 61 (1987) 3763–3765.
[2] L. Schultz, A. El-Aziz, G. Barkleit, K. Mummert, Mater. Sci. Eng. A 267 (1999) 307–313.
[3] K. Tokuhara, S. Hirosawa, J. Appl. Phys. 69 (1991) 5521–5523.
[4] I. Gurappa, J. Alloys Compd. 360 (2003) 236–242.
[5] A. El-Moneim, A. Gebert, M. Uhlemann, O. Gutfleisch, L. Schultz, Corros. Sci. 44 (2002) 1857–1874.
[6] S. Mao, H. Yang, Z. Song, J. Li, H. Ying, K. Sun, Corros. Sci. 1887–1894 (2011).
[7] S. Mao, H. Yang, F. Huang, T. Xie, Z. Song, Appl. Surf. Sci. (2011) 3980–3984.
[8] T. Xie, S. Mao, C. Yu, S. Wang, Z. Song, Vacuum (2012) 1583–1588.
[9] Y. Cheng, X. Pang, K. Gao, H. Yang, A.A. Volinsky, Thin Solid Films 550 (2014) 428–434.
[10] S.Q. Hu, K. Peng, E. Chen, H. Chen, J. Mater. Eng. Perform. 24 (2015) 1–6.
[11] J.M. Hu, X.L. Liu, J.Q. Zhang, C.N. Cao, Prog. Org. Coat. (2006).
[12] X. Ding, X.-C. Wang, K.-H. Ding, S.-L. Cui, Y.-C. Sun, M.-S. Li, Rare Metals (2015) 1–5.
[13] C.B. Ma, F.H. Cao, Z. Zhang, J.Q. Zhang, Appl. Surf. Sci. 253 (2006) 2251–2256.
[14] X.K. Yang, Q. Li, J.Y. Hu, X.K. Zhong, S.Y. Zhang, J. Appl. Electrochem. 40 (2010) 39–47.
[15] W. He, L. Zhu, H. Chen, H. Nan, W. Li, H. Liu, Y. Wang, Appl. Surf. Sci. 279 (2013) 416–423.
[16] Z.C. Zhong, J.L. Xu, Z.X. Huang, J.M. Luo, Rare Metals 33 (2014) 703–708.
[17] S. Wang, W. Li, D. Han, H. Liu, L. Zhu, RSC Adv. 5 (2015) 81759–81767.
[18] A. Saliba-Silva, R.N. Faria, M.A. Baker, I. Costa, Surf. Coat. Technol. 185 (2004) 321–328.
[19] X. Ding, X.C. Wang, K.H. Ding, S.L. Cui, Y.C. Sun, M.S. Li, Rare Metals (2015) 1–5.
[20] S.T. Takeuchi, D. Azambuja, I. Costa, Surf. Coat. Technol. 201 (2006) 3670–3675.
[21] J. Robertson, Materials Science and Engineering: R: Reports, 2002 129–281.
[22] A. Grill, Diam. Relat. Mater. 8 (1999) 428–434.
[23] P. Maguire, J. McLaughlin, T. Okpalugo, P. Lemoine, P. Papakonstantinou, E. McAdams, M. Needham, A. Ogwu, M. Ball, G. Abbas, Diam. Relat. Mater. 14 (2005) 1277–1288.
[24] H.-G. Kim, S.-H. Ahn, J.-G. Kim, S.J. Park, K.-R. Lee, Diam. Relat. Mater. 14 (2005) 35–41.
[25] G. Huang, Z. Lingping, H. Weiqing, Z. Lihua, L. Shaolu, L. Deyi, Diam. Relat. Mater. 12 (2003) 1406–1410.
[26] G. Wu, L. Sun, W. Dai, L. Song, A. Wang, Surf. Coat. Technol. 204 (2010) 2193–2196.
[27] A. Anders, Handbook of Plasma Immersion Ion Implantation and Deposition, Wiley, New York, 2000 etc.
[28] G. Wu, X. Zhang, Y. Zhao, J.M. Ibrahim, G. Yuan, P.K. Chu, Corros. Sci. 78 (2014) 121–129.
[29] Y. Liu, L. Li, X. Cai, Q. Chen, M. Xu, Y. Hu, T.-L. Cheung, C. Shek, P.K. Chu, Thin Solid Films 493 (2005) 152–159.
[30] A.C. Ferrari, J. Robertson, Phys. Rev. B 61 (2000) 14095.
[31] A.C. Ferrari, J. Robertson, Phys. Rev. B (2001) 075414.
[32] A.C. Ferrari, Diamond Relat, Mater. 1053–1061 (2002).
[33] A.C. Ferrari, J. Robertson, Phil. Trans. R. Soc. A (2004) 2477–2512.
[34] Y. Lifshitz, Diam. Relat. Mater. 388–400 (1996).
[35] Y. Lifshitz, S.R. Kasi, J.W. Rabalais, Phys. Rev. Lett. (1989) 1290–1293.
[36] Y. Liu, L. Li, M. Xu, Q. Chen, Y. Hu, X. Cai, P.K. Chu, Surf. Coat. Technol. 200 (2006) 2672–2678.
[37] V. Bellido-Gonzalez, N. Stefanopoulos, F. Deguilhen, Surf. Coat. Technol. 74 (1995) 884–889.
[38] S. Zhang, D. Sun, Y. Fu, H. Du, Surf. Coat. Technol. 198 (2005) 74–84.
[39] C. Liu, Q. Bi, A. Leyland, A. Matthews, Corros. Sci. 45 (2003) 1257–1273.
[40] Y. Xin, T. Hu, P.K. Chu, Corros. Sci. 53 (2011) 1522–1528.
[41] M.I. Jamesh, G. Wu, Y. Zhao, W. Jin, D.R. McKenzie, M.M. Bilek, P.K. Chu, Corros. Sci. 86 (2014) 239–251.
[42] G.-L. Song, Z. Xu, Corros. Sci. 63 (2012) 100–112.
[43] G. Wu, W. Dai, H. Zheng, A. Wang, Surf. Coat. Technol. 205 (2010) 2067–2073.
[44] L.A. Zepeda-Ruiz, G.H. Gilmer, C.C. Walton, A.V. Hamza, E. Chason, J. Cryst. Growth 312 (2010) 1183–1187.
[45] A. Kim, F. Camp, T. Lizzi, J. Appl. Phys. 79 (1996) 4840–4842.
[46] A.A. El-Moneim, A. Gebert, M. Uhlemann, O. Gutfleisch, L. Schultz, Corros. Sci. 44 (2002) 1857–1874.
[47] G. Yan, A. Williams, J. Farr, I. Harris, J. Alloys Compd. 292 (1999) 266–274.
[48] J.J. Li, A.H. Li, M.G. Zhu, W. Pan, W. Li, J. Appl. Phys. (2011) 07A744.